Supplementary Information
Chemical Control of Competing Electron Transfer Pathways in Iron Tetracyano-Polypyridyl Photosensitizers

Kristjan Kunnus, Lin Li, Charles J. Titus, Sang Jun Lee, Marco E. Reinhard, Sergey Koroidov, Kasper S. Kjær, Kiryong Hong, Kathryn Ledbetter, William B. Doriese, Galen C. O'Neil, Daniel S. Swetz, Joel N. Ullom, Dale Li, Kent Irwin, Dennis Nordlund, Amy A. Cordones, Kelly J. Gaffney

Global analysis of the UV-Visible transient absorption data

UV-Visible transient absorption data was analyzed by means of global fitting procedure based on singular value decomposition (SVD).[1] We follow here a procedure that has become a standard in the analysis 2-variable transient absorption data (see e.g. Supplementary Information of Gawelda *et al.*[2]). Briefly, SVD decomposes a 2-variable data matrix into column vectors U and row vectors V that in current context correspond to basis difference spectra and basis time traces (kinetics). Each pair of U and V is associated with a singular value S that represents a weight of these components. Typically, a few U/V pairs describe majority of the kinetics, as indicated by significantly higher S value, while the rest of U/V pairs primarily contain noise. Here, depending on the noise level, we use only the first or two first row vector(s) V to analyze the kinetics. The results of this global analysis are shown in Fig. S1-S3. For each data set we display the first three S values and V vectors to show that only the first two contain signal. The selected V vectors are fitted simultaneously with either a two-component sequential (**1** and **2** in H_2O and MeOH) or parallel exponential kinetics (all the rest). Kinetics traces are convoluted with a Gaussian temporal instrument response function (IRF). Thus, the j-th V vector is fitted with:

$$V^j(t) = \sum_{i=1}^{2} I_i^j \, P_i(t)$$

Where I_i^j is the intensity of the i-th component with a time dependence of $P_i(t)$. In the case of sequential kinetics:

$$P_1(t) = 0.5exp(k_1(t_0 - t) + 0.5(k_1c)^2)\left[1 + erf\left(\frac{t - t_0 - k_1c^2}{\sqrt{2}c}\right)\right]$$

$$P_2(t) = 0.5\frac{k_1}{k_2 - k_1}exp(k_1(t_0 - t) + 0.5(k_1c)^2)\left[1 + erf\left(\frac{t - t_0 - k_1c^2}{\sqrt{2}c}\right) - exp(k_2(t_0 - t) + 0.5(k_2c)^2)\left(1 + erf\left(\frac{t - t_0 - k_2c^2}{\sqrt{2}c}\right)\right)\right]$$

In case of parallel kinetics both components have the same functional form:

$$P_i(t) = 0.5exp(k_i(t_0 - t) + 0.5(k_ic)^2)\left[1 + erf\left(\frac{t - t_0 - k_ic^2}{\sqrt{2}c}\right)\right]$$

Here $k_i = 1/\tau_i$ is the rate constant, t_0 is time-zero and $c = FWHM/\left(2\sqrt{2ln(2)}\right)$ is the standard deviation of the IRF (in all the measurements t_0 = 0 fs and FWHM = 100 fs). Respective species associated spectra (SAS) of the i-th component are calculated as

$$SAS_i(\lambda) = \sum_{j=1}^{2} S^j I_i^j \, U^j(\lambda)$$

The faster component in parallel fits can be assigned to cooling/solvation of the ^{3}MLCT state or, more likely in some cases, to a residual cross phase modulation artefact (data before 100 – 200 fs is excluded in all the fits due to cross phase modulation).

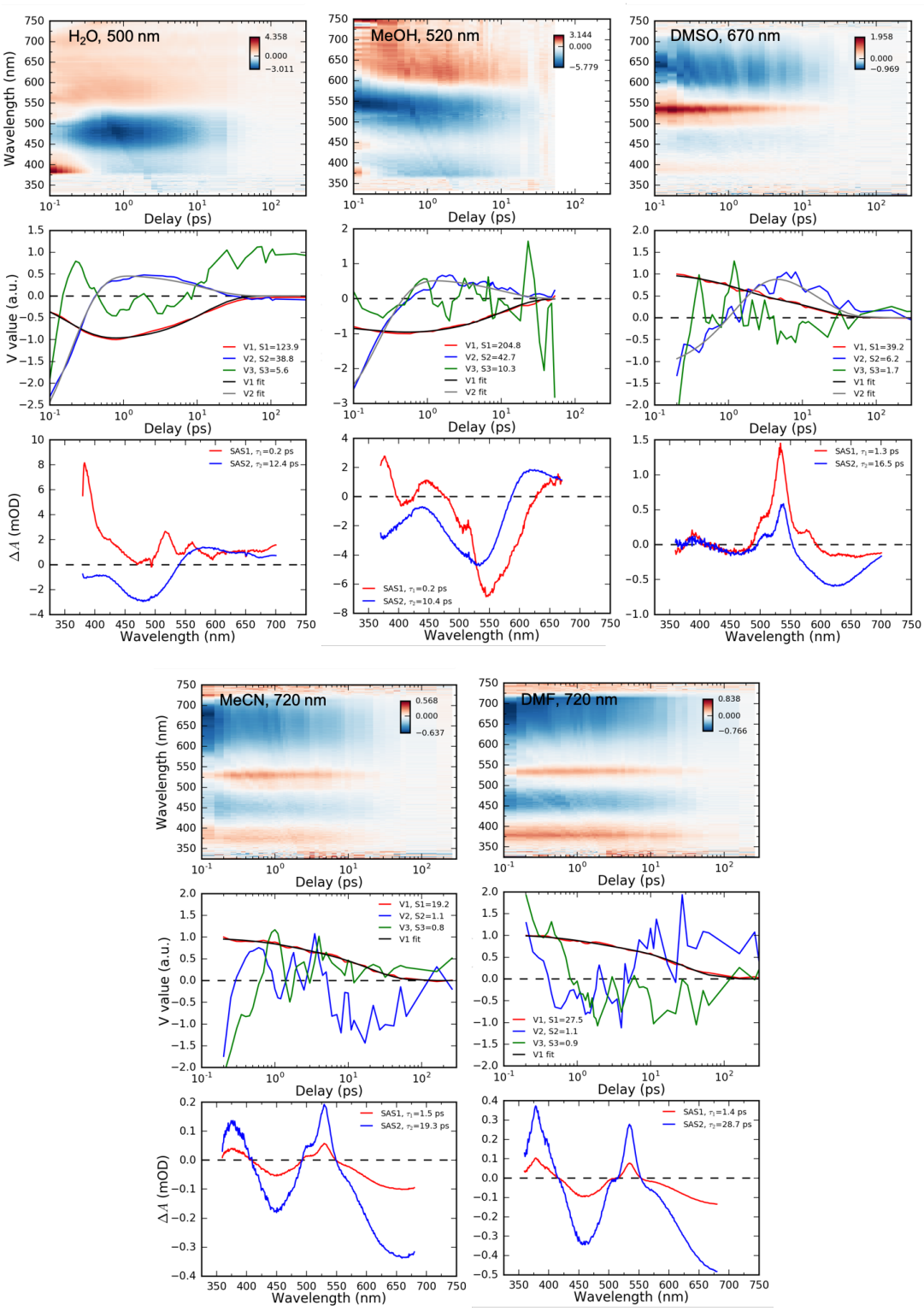

Fig. S1. Results of global fitting of transient UV-Visible absorption data of complex **1**. For each measurement is shown a map with time dependence of difference UV-Visible spectra, time evolution of first three SVD components and the resulting species associated difference spectra. Kinetic model is sequential in H2O and MeOH solvents and parallel in other solvents (with faster component assigned to cooling/solvation of ^{3}MLCT).

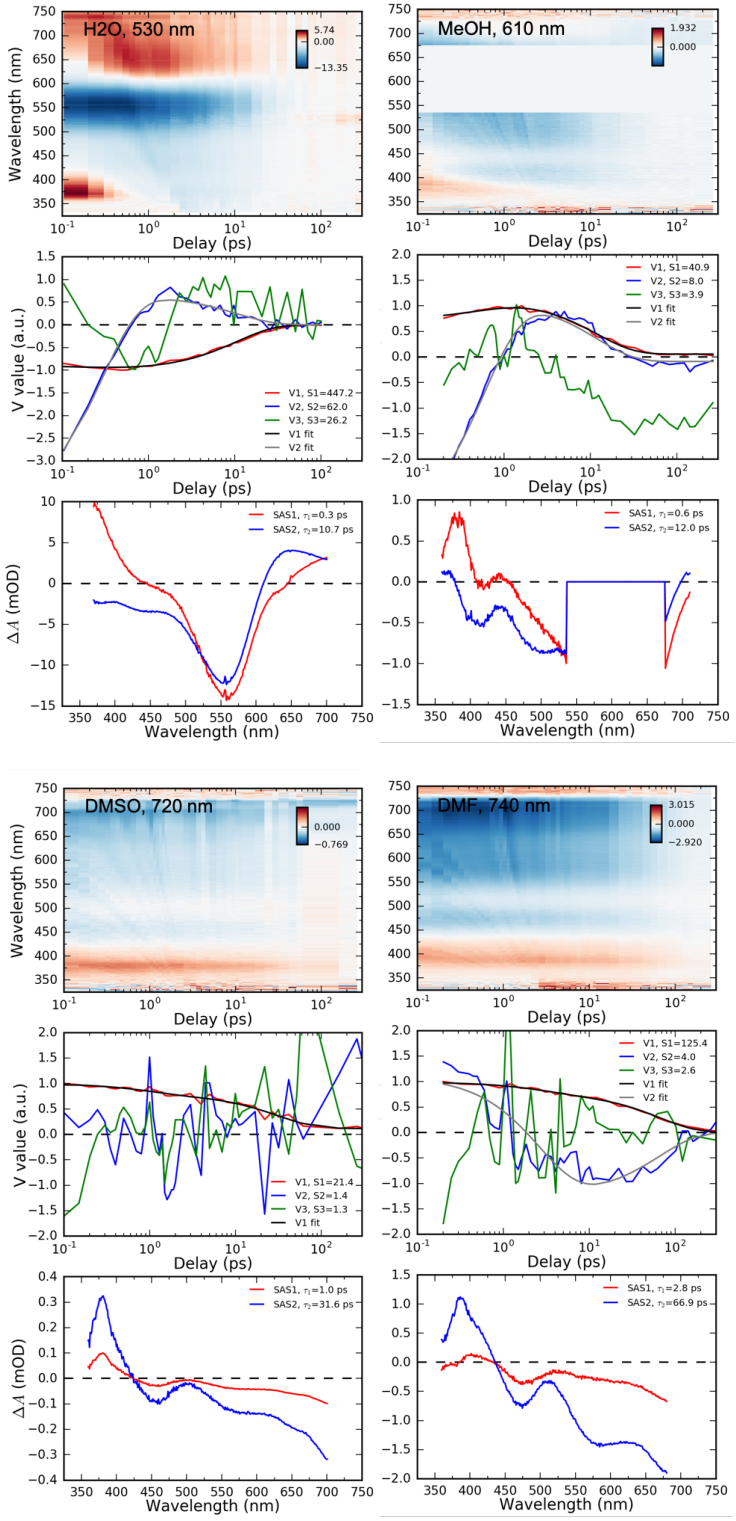

Fig. S2. Results of global fitting of transient UV-Visible absorption data of complex **2**. For each measurement is shown a map with time dependence of difference UV-Visible spectra, time evolution of first three SVD components and the resulting species associated difference spectra. Kinetic model is sequential in H2O and MeOH solvents and parallel in other solvents (with faster component assigned to cooling/solvation of ^{3}MLCT).

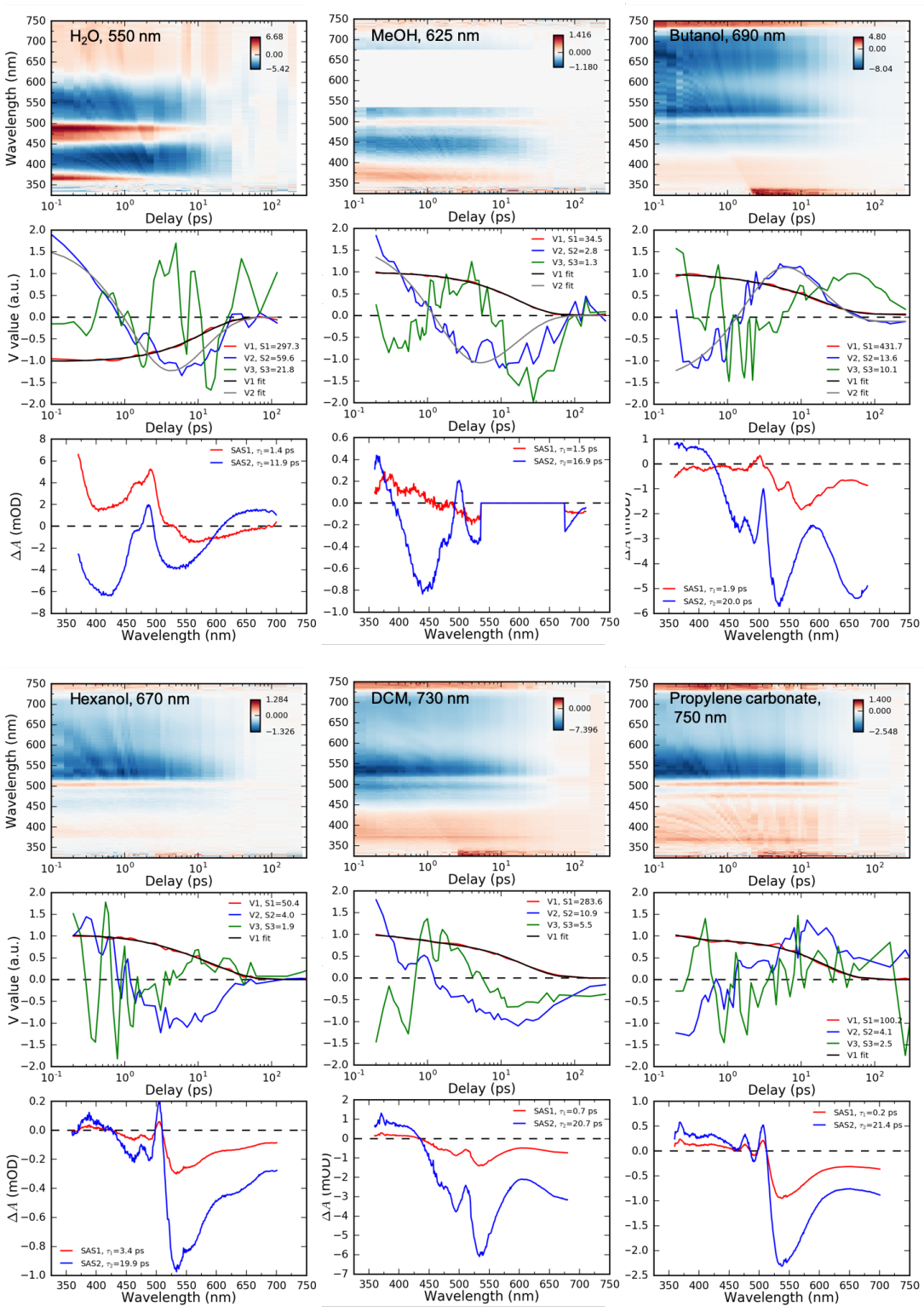

Fig. S3. Results of global fitting of transient UV-Visible absorption data of complex **3**. For each measurement is shown a map with time dependence of difference UV-Visible spectra, time evolution of first three SVD components and the resulting species associated difference spectra. Kinetic model is parallel in all the solvents (with faster component assigned to cooling/solvation of ^{3}MLCT).

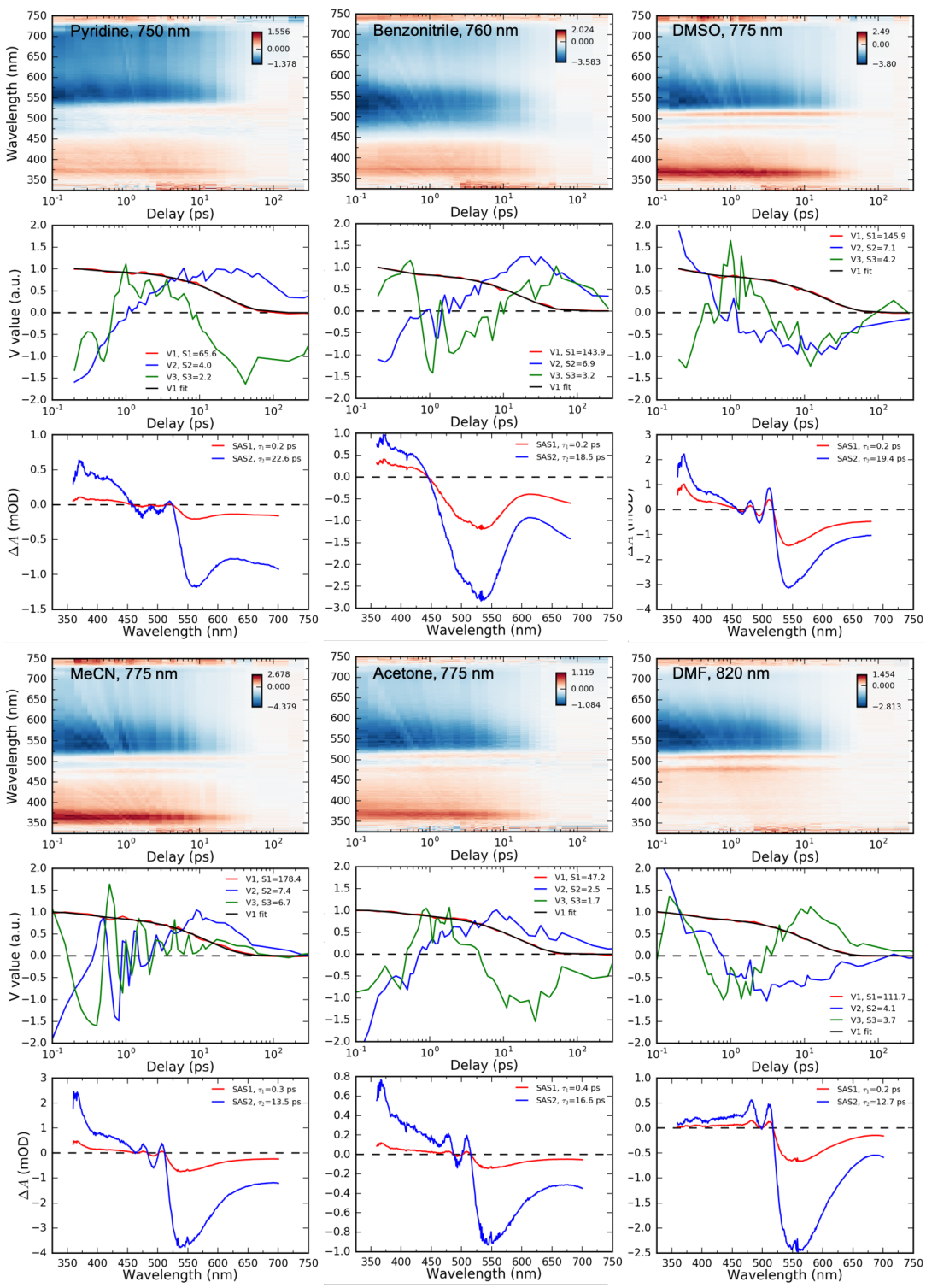

Fig. S3. (Continued)

Fits of the UV-Visible absorption spectra

UV-Visible absorption spectra of complexes **1**, **2** and **3** in all the investigated solvents are shown in Fig. S4-S6. Lowest energy ^{1}MLCT and ^{3}MLCT peaks are fitted with a vibronic peak shape function described in the main manuscript. The higher energy MLCT band is fitted with two Gaussians (shown as a single peak for **1** and **3**).

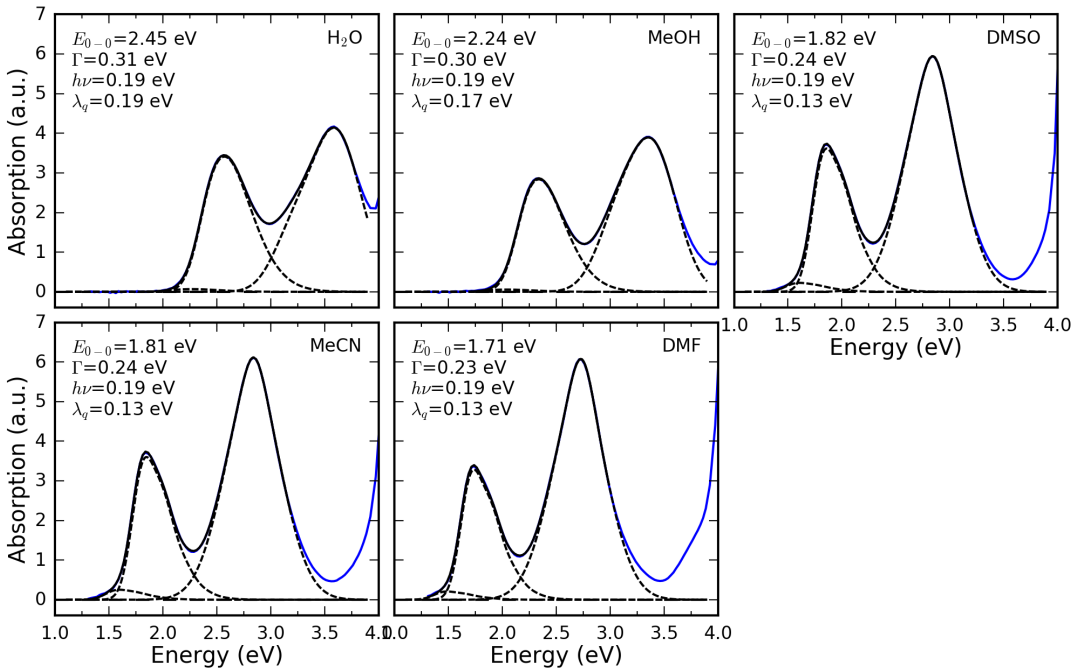

Fig. S4. Peak fitting of the UV/vis spectra of complex **1** in various solvents. Optimal fit parameters of the lowest energy ^{1}MLCT absorption band are shown on the respective panels. Blue line – data, black line – fit, dashed line – individual peaks from the fit. MeOH – methanol, DMSO – dimethylsulfoxide, MeCN – acetonitrile, DMF – dimethylformamide.

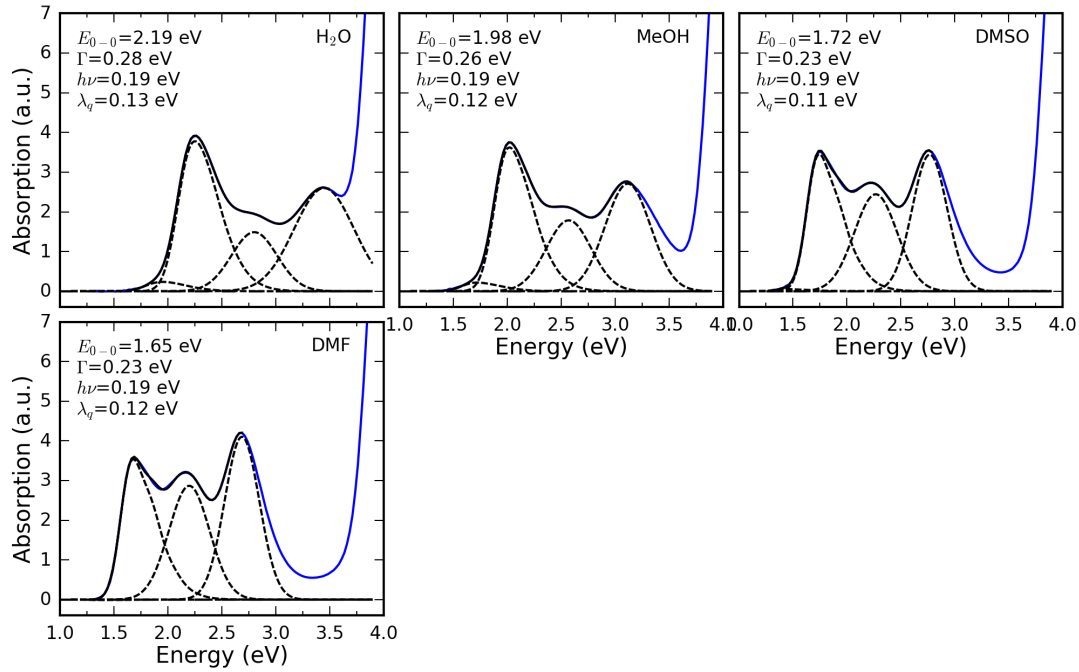

Fig. S5. Peak fitting of the UV/vis spectra of complex **2** in various solvents. Optimal fit parameters of the lowest energy ^{1}MLCT absorption band are shown on the respective panels. Blue line – data, black line – fit, dashed line – individual peaks from the fit. MeOH – methanol, DMSO – dimethylsulfoxide, DMF – dimethylformamide.

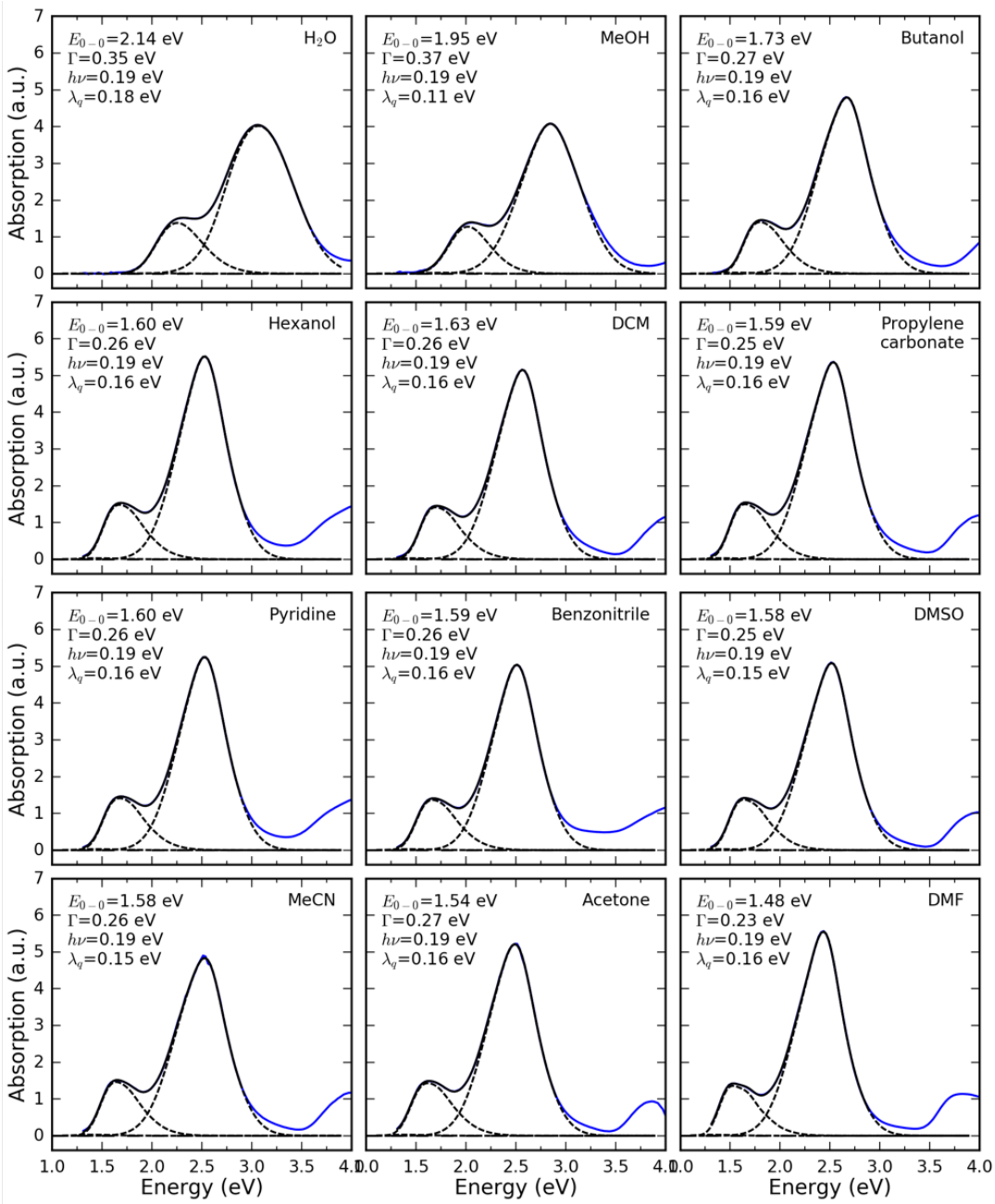

Fig. S6. Peak fitting of the UV/vis spectra of complex **3** in various solvents. Optimal fit parameters of the lowest energy ^{1}MLCT absorption band are shown on the respective panels. Blue line – data, black line – fit, dashed line – individual peaks from the fit. MeOH – methanol, DCM – dichloromethane, DMSO – dimethylsulfoxide, MeCN – acetonitrile, DMF – dimethylformamide.

Results of the DFT calculations

Density functional theory (DFT) and time-dependent (TD) DFT calculation of complexes **1**, **2** and **3** where carried out using the ORCA 4.1.0 version.[3] All calculations were performed at the B3LYP level[4,5] with def2-TZVP basis set[6], including the geometry optimization. This level of calculation has been shown to match the experimental Fe-ligand bond lengths for these complexes within errors of 3%.[7] The effect of DMF solvent was included using the conductor-like polarizable continuum model (CPCM).[8] Input files of the calculations are included in the next section. Comparison of relevant frontier molecular orbitals (MOs) is in Table S1 and comparison of lowest energy electronic excitations to the ^{1}MLCT states is presented in Table S2.

Table S1. Energies of calculated DFT frontier MOs from HOMO-2 to LUMO+2 for complexes **1**, **2** and **3**.

MO		**1**		**2**		**3**	
type	GS occ.	Num.	E (eV)	Num.	E (eV)	Num.	E (eV)
Fe t_{2g}	2	78	-4.9286	98	-5.1298	78	-5.1105
Fe t_{2g}	2	79	-4.8236	99	-5.0216	79	-5.0034
Fe t_{2g}	2	80	-4.7592	100	-4.9573	80	-4.9450
L π^*	0	81	-1.7327	101	-2.0940	81	-2.1209
L π^*	0	82	-0.9362	102	-1.5696	82	-1.4864
L π^*	0	83	-0.6882	103	-1.0245	83	-1.2744

Table S2. Calculated TDDFT electronic dipole transitions corresponding to the three lowest energy singlet excited states for complexes **1**, **2** and **3**. All transitions are of type GS->^{1}MLCT (Fe t_{2g} -> L π^*), where L is the polypyridyl ligand. f is oscillator strength.

1			**2**			**3**		
Trans.	E (eV)	f	Trans.	E (eV)	f	Trans.	E (eV)	f
80->81	1.761	0.001	100->101	1.560	0.001	80->81	1.550	0.000
78->81	1.877	0.000	98->101	1.675	0.000	78->81	1.666	0.000
79->81	2.111	0.040	99->101	2.013	0.038	79->81	1.843	0.023

Input files of the DFT calculations

ORCA input file for the calculation of complex **1**:

```
! B3LYP 6-311G** RIJCOSX Grid5 FinalGrid6 CPCM(DMF) TightSCF PAL8
%basis newgto
Fe "def2-TZVP"
end
end
%maxcore 1000
%tddft
  maxdim 5
  nroots 20
end
*xyz -2 1
C   -0.00155733545947     0.35342675075218    -2.64387773466127
C    0.00218308686649     1.46699816586904    -3.47366703655545
C    0.00176643969400     0.35239465353084     2.64150167796138
C   -0.00013543364881     1.67186277312580     0.73591624754990
C    0.00114030853150     1.67216137917836    -0.73777787501089
```

```
C   0.00578192738431     2.83628094941793    -1.51201551065051
C   -0.00411484850045    2.83569388514102     1.51058289228139
C   -0.00473892691161    2.73385916598340     2.89539247206001
C   -0.00132664062296    1.46567150494627     3.47170788806511
C   0.00630787153935     2.73496850548130    -2.89686898939695
N   -0.00180416261446    0.44095046320738    -1.30398222900019
N   0.00203926644537     0.44044056254543     1.30165538103244
H   -0.00782711401430    3.80861531955052     1.03794128734041
H   -0.00789690546626    3.62574406707555     3.51075919499425
H   0.00368326733489    -0.65152481836864     3.04484741081482
H   0.00243546796081     1.33444087217167    -4.54851092953674
H   -0.00166299437548    1.33271079692330     4.54650120526781
H   0.01004448013724     3.80902241902772    -1.03901027036795
H   0.00993456178428     3.62708022812698    -3.51190287668829
H   -0.00407707782940    -0.65034941227889    -3.04759574927524
Fe  -0.00060194772181    -1.12444526305113    -0.00141804806918
C   -0.00516140492155    -2.48525080256576    -1.37885147136791
C   1.96816072476673     -1.13341650879356    -0.00445192793919
N   3.13720873138036     -1.12500179238312     0.00190274920811
N   -0.00651122349618    -3.29301331709356    -2.22590826564015
C   -1.96932756012783    -1.13143568302471     0.00760462004510
C   0.00286435194268     -2.48577439139554     1.37530551891654
N   -3.13829875813679    -1.12208294762188     0.02221417236409
N   0.00411284807934     -3.29390652547790     2.22200619625856
```

ORCA input file for the calculation of complex **2**:

```
! B3LYP 6-311G** RIJCOSX Grid5 FinalGrid6 TightSCF CPCM(DMF) PAL8
%basis newgto
Fe "def2-TZVP"
end
end
%maxcore 1000
%tddft
  maxdim 5
  nroots 20
end
*xyz -2 1
C   2.55018699630380     0.48337162026129     0.42813500942915
C   3.17332296516988    -0.74408352800326     0.59739221560112
C   -2.63853045366711    1.21297023767461     0.10391167012618
C   -0.95926960422898   -0.37198267149965     0.34938722313207
C   0.50136018547224    -0.58600312592998     0.31941730127430
C   1.17568045869000    -1.82565754112148     0.33534362149612
C   -1.90157226304395   -1.34527691116769     0.69779312856192
C   -3.25048172947971   -1.01560000843683     0.71991165266470
C   -3.62836323847379    0.28436199660680     0.39722345155636
N   2.50046955381753    -1.89335889389216     0.51359729702853
N   1.22122433111233     0.56676729303695     0.28706643476199
N   -1.33193252562439    0.90721705679886     0.09287705877949
H   -1.58797937222941   -2.34102841284302     0.97042438578826
H   -3.98879759486486   -1.76074601252121     0.99095828469059
H   -2.88013125218006    2.24358007296862    -0.11883845116460
H   4.24325271629648    -0.80039736002737     0.76661362474984
H   -4.66769923036644    0.58819810977542     0.39221733358883
H   3.10533542044461     1.41045749315923     0.39582945087229
```

```
Fe  0.18733018511574     2.23868719771254    -0.11640202712334
C   1.75445336289148     3.37133391741698    -0.25007077163109
C   0.32486883842313     1.82781985587368    -2.03700189043669
N   0.40248662695719     1.56748051130284    -3.17339913296609
N   2.70759121837906     4.04491384048849    -0.32637714402161
C   0.03991660004263     2.69615741307981     1.79305447037968
C   -0.95797860350595    3.74352400895319    -0.54750021906166
N   -0.04827036152398    2.95967810188690     2.92791614699323
N   -1.66055863681632    4.64237522834678    -0.80492695374915
C   0.52260630566481    -3.14624770255306     0.06336226508049
C   -0.07007492967673   -3.38875624530935    -1.17908457364267
C   -0.59512278376784   -4.65229067823617    -1.43219072544159
C   -0.51685138309856   -5.62187895510922    -0.43604186139199
C   0.09430690245055    -5.28495706603209     0.77007220257274
N   0.61364719955707    -4.07697522952190     1.02477267392878
H   -0.10935715978643   -2.60735623265271    -1.92875259986434
H   -1.05356805377028   -4.87398564558876    -2.38909184942086
H   -0.91465908852121   -6.61830271666350    -0.58611911836257
H   0.17315018783745    -6.01692879823357     1.56873687522158
```

ORCA input file for the calculation of complex **3**:

```
! B3LYP 6-311G** RIJCOSX Grid5 FinalGrid6 TightSCF CPCM(DMF) PAL8
%basis newgto
Fe "def2-TZVP"
end
end
%maxcore 1000
%tddft
  maxdim 5
  nroots 20
end
*xyz -2 1
C   0.00163035028385     2.64122668870430     0.38822965896693
C   -0.00039442576891    3.41048701654237     1.54115405051362
C   0.00118342104328    -2.64089712866631     0.38836545672200
C   0.00046460456738    -0.73971498648915     1.67240583314859
C   -0.00052968838893    0.73993721216228     1.67221359606585
N   -0.00347381315472    1.40126714786476     2.82701620700737
N   0.00079663823569    -1.40099553178771     2.82740767082186
C   0.00092572080744    -2.73482315307915     2.75860533793085
C   0.00110423989192    -3.41017616904772     1.54124766942692
C   -0.00338402731446    2.73505374930415     2.75845048962468
N   0.00130245158788     1.29897001443523     0.44221060461743
N   0.00080511891524    -1.29869921062685     0.44239286083295
H   0.00029808623430    -3.27251522174274     3.70132364011692
H   0.00129326135701    -3.07886985548369    -0.60127435946120
H   0.00001522636642     4.49123944592669     1.49061778727868
H   0.00112716674689    -4.49093011050629     1.49058895945695
H   -0.00613137792420    3.27258544426457     3.70126412670238
H   0.00361404575672     3.07920274345014    -0.60139344578751
Fe  0.00048718220976     0.00020601414139    -1.11717118427401
C   0.00188572323541     1.38669433345868    -2.46894165046937
C   -1.96938477333487    0.00108661337607    -1.13769216662903
N   -3.13773727464004    0.00089276494748    -1.13990715459186
N   0.00336597694827     2.23957700428695    -3.26950961117986
```

C	1.97002112859246	-0.00204204135615	-1.14031330313842
C	-0.00269328982102	-1.38614505976550	-2.46894974234980
N	3.13839768911114	-0.00378947553380	-1.14607916052368
N	-0.00498936154394	-2.23882824878002	-3.26964364082925

Analysis of the Fe 2p3d RIXS spectra

Fig. S7 displays the X-ray absorption spectra (XAS) and RIXS spectra of complexes **1**, **2** and **3**. RIXS spectra were measured at the Fe L_3-edge e_g-resonance (black sticks on the Fig. S7). The dominant RIXS feature corresponds to a MC final state, with the intensity at higher energy transfer >5 eV belonging mostly to the ^{1}LMCT final states.[9] In addition, the resonant elastic scattering ($^1A_{1g}$ GS final state) peak is visible at 0 eV. In order to assign the dominant MC RIXS feature at ~3 eV, we inspect the energy terms corresponding to the MC states. Out of 43 total terms of a $3d^6$ configuration in an octahedral ligand field, only four terms correspond to a single $t_{2g}\rightarrow e_g$ orbital excitation (with respect to the ground state $^1A_{1g}$ t_{2g}^6) and can thus contribute intensity to the MC RIXS features. Terms corresponding to multi-electron excitations can have intensities only due to mixing with the single-electron excited states, therefore, these final states intensities are generally small (also they overlap energetically with the LMCT states). Two of the four terms are spin singlets, $^1T_{1g}$ and $^1T_{2g}$, and two are spin triplets, $^3T_{1g}$ and $^3T_{2g}$. The former two have the same spin multiplicity as the ground state ($^1A_{1g}$). Because the intermediate core-excited states T_{1u} symmetry has better overlap with T_{1g} than with T_{2g}, the $^1T_{1g}$ final state dominates the MC RIXS spectrum. The latter two have different spin multiplicity from the ground state and therefore only gain RIXS intensity due to the 2p spin-orbit interaction (ξ_{2p} ~ 7 eV) in the core-hole excited intermediate state that causes the e_g-resonance to have slightly mixed singlet-triplet spin character. The dominant features in the smaller intensity shoulders due to the $^1T_{2g}$, $^3T_{1g}$ and $^3T_{2g}$ states are also observed. The above considerations have been corroborated by ~1 eV resolution RIXS experiments and ab-initio simulations of $K_4[Fe(CN)_6]$ in H_2O[9] and recent ~0.3 eV resolution experiments on solid $K_4[Fe(CN)_6]$.[10]

Given the modest resolution of the RIXS spectra measured with the TES spectrometer, we resolve only the dominant $^1T_{1g}$ MC RIXS feature (Fig. S7). In order to confirm that the maximum position of this RIXS feature can be reliably associated with the energy of the $^1T_{1g}$ state we carried out a peak fitting procedure described below. Whole RIXS spectrum is fitted with six peaks: $^1A_{1g}$ (elastic peak, position fixed at 0 eV), $^3T_{1g}$, $^1T_{1g}$, $^1T_{2g}$ and two ^{1}LMCT peaks (shown as one in Fig. S7). The shapes of the elastic peak and the MC peaks were fixed to an asymmetric TES spectral response measured at 750 eV (Fig. S3A). This is possible because the 2.3 eV FWHM TES resolution is by far the largest contribution to the width of the RIXS peaks (intrinsic FWHM is ~0.5 eV or smaller). Additional gaussian broadening is included for the ^{1}LMCT peak (described with a sum of two peaks). The energies of the MC states are not independent but determined by an octahedral ligand field 10Dq and two 3d electron repulsion Racah parameters B and C (for reference, we have printed the relevant Tanabe-Sugano matrices in the next section).[11,12] B and C values are known with a good accuracy. In compounds containing 3d metal ions with coordinative bonds, the values of B and C are 70% – 80% of the atomic Hartree-Fock values.[13,14] To accurately determine the scaling factor for B and C, and to determine the relative intensities of the weak $^3T_{1g}$ and $^1T_{2g}$ states with respect to $^1T_{1g}$, we fit a higher-resolution RIXS spectrum of **1** from Ref. [15] (Fig. S8B). The two times better energy resolution (~1 eV) in Ref. [15] enables us to resolve the weak $^3T_{1g}$ and $^1T_{2g}$ peaks more clearly than it is possible with the present TES RIXS measurement. This fit of the positions of $^3T_{1g}$ and $^1T_{1g}$ indicates that the scaling of B and C is 75% (B = 0.110 eV and C = 0.406 eV). Now, by fixing the scaling factor and relative intensities of $^1T_{1g}$, $^3T_{1g}$ and $^1T_{2g}$ to values retrieved from fitting the RIXS spectrum from Ref. [15], we fit the TES RIXS spectra of **1**, **2** and **3** with only two free parameters for the MC states: 10Dq and intensity of the $^1T_{1g}$ peak (Fig. S7).

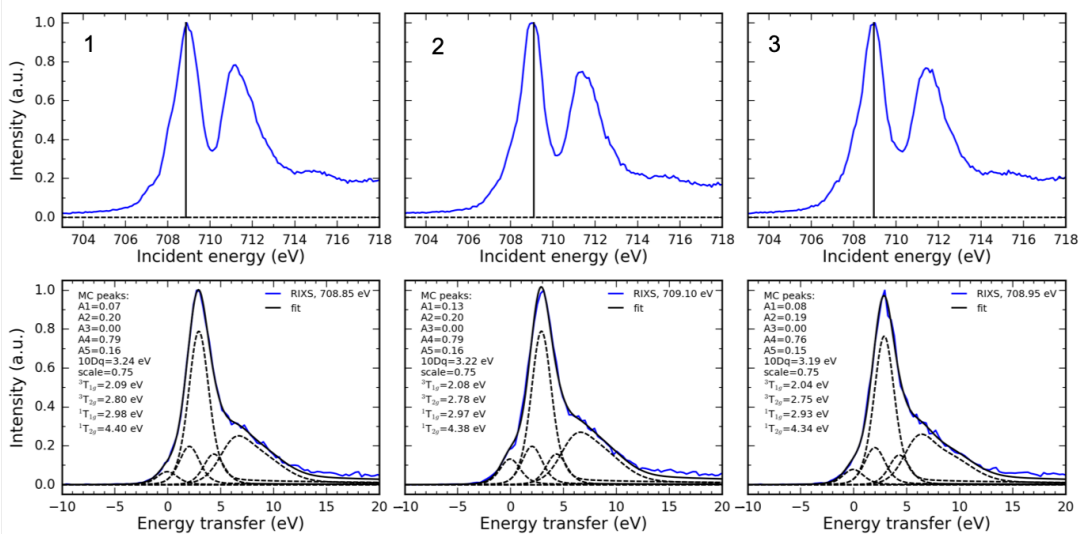

Fig. S7. XAS and RIXS spectra of complexes **1**, **2** and **3**. Top row: partial fluorescence yield XAS spectra, black stick indicates the white line e_g-resonance where the RIXS spectra were measured. Bottom row: Results of peak fitting of the RIXS spectra. Parameters describing the MC RIXS peaks: A – intensity (1 = elastic peak, 2 = $^3T_{1g}$, 3 = $^3T_{2g}$, 4 = $^1T_{1g}$, 5 = $^1T_{2g}$), 10Dq – octahedral ligand field, scale – scaling factor of Racah parameters B and C. MC states energies are calculated based on Tanabe-Sugano matrices (see next section).

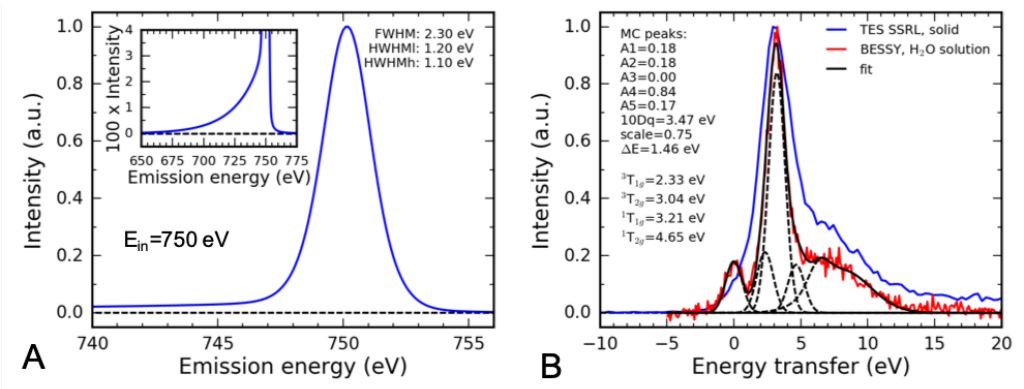

Fig. S8. (A) Spectral response on the SSRL TES spectrometer measured using monochromatic elastically scattered 750 eV photons (HWHMl – low energy side half-width at half-maximum, HWHMh – high energy side half-width at half-maximum). (B) Comparison of RIXS spectra of complex **1** measured using the SSRL TES spectrometer and Nordgren-type grating spectrometer at BESSY-II (From Jay *et al.*[9]). Parameters describing the MC RIXS peaks: A – intensity (1 = elastic peak, 2 = $^3T_{1g}$, 3 = $^3T_{2g}$, 4 = $^1T_{1g}$, 5 = $^1T_{2g}$), 10Dq – octahedral ligand field, scale – scaling factor of Racah parameters B and C, ΔE – Gaussian FWHM of the peaks. MC states energies are calculated based on Tanabe-Sugano matrices (see next section).

Tanabe-Sugano matrices of d^6 ion

The MC state energies of complexes **1**, **2** and **3** are given by diagonalization of the d^6 configuration Tanabe-Sugano matrices. Below are shown the matrices for the symmetries that include the low energy MC states relevant for this work (a constant term 15A in the diagonal is omitted, matrices are symmetric and only the elements above the diagonal are printed).[11,12] A, B and C are the Racah parameters describing the electrostatic repulsion between the 3d electrons (only B and C are relavant for the relative energetics of the MC states). 10Dq is the conventional parameter describing octahedral ligand field.

$^1A_{1g}$:

$$\begin{vmatrix} 16Dq + 10C & -12\sqrt{2}B & \sqrt{2}(4B + 2C) & 2\sqrt{2}B & 0 \\ & 6Dq + 6C & -12B & -6B & 0 \\ & & -4Dq + 14B + 11C & 20B & \sqrt{6}(2B + C) \\ & & & -4Dq - 3B + 6C & 2\sqrt{6}B \\ & & & & -24Dq - 16B + 8C \end{vmatrix}$$

$^3T_{1g}$:

$$\begin{vmatrix} 16Dq - 15B + 10C & -\sqrt{6}B & -3\sqrt{2}B & \sqrt{2}(2B + C) & -2\sqrt{2}B & 0 & 0 \\ & 6Dq - 11B + 4C & 5\sqrt{3}B & \sqrt{3}B & -\sqrt{3}B & 3B & \sqrt{6}B \\ & & 6Dq - 3B + 6C & -3B & -3B & 5\sqrt{3}B & \sqrt{2}(B + C) \\ & & & -4Dq - B + 6C & -10B & 0 & 3\sqrt{2}B \\ & & & & -4Dq - 9B + 4C & -2\sqrt{3}B & -3\sqrt{2}B \\ & & & & & -4Dq - 11B + 4C & \sqrt{6}B \\ & & & & & & -14Dq - 16B + 5C \end{vmatrix}$$

$^1T_{2g}$:

$$\begin{vmatrix} 16Dq - 9B + 7C & 3\sqrt{2}B & -5\sqrt{6}B & 0 & -2\sqrt{2}B & \sqrt{2}(2B + C) & 0 \\ & 6Dq - 9B + 6C & -5\sqrt{3}B & 3B & -3B & -3B & -\sqrt{6}B \\ & & 6Dq + 3B + 8C & -3\sqrt{3}B & 5\sqrt{3}B & -5\sqrt{3}B & \sqrt{2}(3B + C) \\ & & & -4Dq - 9B + 6C & -6B & 0 & -3\sqrt{6}B \\ & & & & -4Dq - 3B + 6C & -10B & \sqrt{6}B \\ & & & & & -4Dq + 5B + 8C & \sqrt{6}B \\ & & & & & & -14Dq + 7C \end{vmatrix}$$

$^3T_{2g}$:

$$\begin{vmatrix} 6Dq - 9B + 4C & -5\sqrt{3}B & \sqrt{6}B & \sqrt{3}B & -\sqrt{2}B \\ & 6Dq - 5B + 6C & -3\sqrt{2}B & 3B & \sqrt{2}(3B + C) \\ & & -4Dq - 13B + 4C & -2\sqrt{2}B & -6B \\ & & & -4Dq - 9B + 4C & 3\sqrt{2}B \\ & & & & -14Dq - 8B + 5C \end{vmatrix}$$

$^1T_{1g}$:

$$\begin{vmatrix} 6Dq - 3B + 6C & 5\sqrt{3}B & 3B & \sqrt{6}B \\ & 6Dq - 3B + 8C & -5\sqrt{3}B & \sqrt{2}(B + C) \\ & & -4Dq - 3B + 6C & -\sqrt{6}B \\ & & & -14Dq - 16B + 7C \end{vmatrix}$$

Fits of the reorganization energy trends

Dependence of classical and high-frequency mode reorganization energies from the ^{1}MLCT minimum energy $E_0^{(^1MLCT)}$ in Fig. 4 were fitted with a linear model: $\lambda = aE_0^{(^1MLCT)} + b$. Linear model was fitted to the data using orthogonal distance regression to account for uncertainties in both reorganization energies and $E_0^{(^1MLCT)}$. Table S3 summarizes the fitting results.

Table S3. Linear fitting results of the reorganization energies dependence from the ^{1}MLCT minimum energy. Linear model parameters: a – slope, b – intercept. Data and fitting results are shown in Fig. 4.

Complex	λ_{cl}		λ_q	
	a	b (eV)	a	b (eV)
1	0.26±0.04	-0.22±0.06	0.12±0.01	-0.06±0.02
2	0.22±0.02	-0.13±0.03	0.03±0.02	0.07±0.03
3	0.50±0.06	-0.45±0.09	0.04±0.02	0.10±0.02

Derivation of the Marcus-Jortner rate equation

Below is presented a concise derivation of the Marcus-Jortner rate equation utilized in the main manuscript (Equation (4)). For further details we refer the reader to the book of May and Kühn[16], as well as to the original publications by Marcus, Jortner and Barbara.[17–24]

Fermi's Golden Rule formula of first-order perturbation theory gives a transition rate between two states

$$k = \frac{2\pi|V|^2}{\hbar} D(-\Delta G)\,.$$

In the context of electron transfer, V is non-adiabatic electronic coupling between the reactant and product states and D is temperature-averaged and Frank-Condon weighted density of vibrational states of the product, taken at negative driving force ΔG. V is considered to be a constant quantity (independent of nuclear coordinates). Therefore, the task of formulating an explicit electron transfer rate equation for a given system reduces to finding a proper D of the system. Note that Fermi's Golden Rule formula requires that all vibrational relaxation time scales are faster than any other characteristic electronic ($t_{el} = \hbar/|V|$) or vibrational ($t_{vib} = 1/v$) time scales. The system is therefore in a (quasi)equilibrium during the whole electron transfer process, i.e. populations in both reactant and product follow a thermal distribution. This also means that nuclear coherence (wavepacket dynamics) effects are not included. In addition, we assume that the electron transfer is non-adiabatic, i.e. nuclear motions can be described as taking place on diabatic reactant or product surfaces, which requires that characteristic vibrational motions are faster than electronic dynamics ($t_{el} \gg t_{vib}$).

To find an explicit formula for the density of states D we first do few simplifications: 1) all vibrational modes are considered to be harmonic, 2) identity of vibrational modes is same in reactant and product (no Duschinsky rotation), and 3) vibrational frequencies of reactant and product modes are identical. Vibrational overlaps can be then calculated by multiplying one-dimensional Franck-Condon factors. A sum over vibrational progressions of different modes gives an expression for density of states

$$D(E) = \sum_{i_1} \dots \sum_{i_N} \sum_{f_1} \dots \sum_{f_N} \frac{e^{-\sum_j^N h v_j i_j / k_B T}}{Z} \prod_j^N \left|\langle f_j | i_j \rangle\right|^2 \delta\left(E - \sum_j^N h v_j (f_j - i_j)\right),$$

where i_j and f_j ($j = 1 \dots N$) are initial (reactant) and final (product) states vibration quantum numbers, respectively. N is number of modes, $h\upsilon_j$ is vibration quantum energy and Z is partition function.
Equation (4) includes only two effective vibrational modes ($N = 2$), where one is a quantum mode and other is a classical mode ($h\upsilon \ll k_B T$). The density of states becomes therefore

$$D(E) = \frac{1}{\sqrt{4\pi k_B T \lambda}} \sum_i \sum_f \frac{e^{-h\upsilon i/k_B T}}{Z} |\langle f|i\rangle|^2 exp\left[-\frac{(-E + (f-i)h\upsilon + \lambda)^2}{4\lambda k_B T}\right],$$

where λ is reorganization energy of the classical mode. Because vibrational quantum energy of the quantum mode is significantly larger than thermal energy ($h\upsilon \gg k_B T$), then we can only consider i=0 contributions. Relevant Franck-Condon factors are thus $|\langle f|0\rangle|^2 = S^f e^{-f}/f!$ (S is the Huang-Rhys parameter of the quantum mode) and thermal-averaging over vibrationally excited states of the quantum mode can be removed:

$$D(E) = \frac{1}{\sqrt{4\pi k_B T \lambda}} \sum_f \frac{S^f e^{-S}}{f!} exp\left[-\frac{(-E + fh\upsilon + \lambda)^2}{4\lambda k_B T}\right].$$

Insertion of this density of states to Fermi's Golden Rule formula yields Equation (4):

$$k = k_0 \sum_f \frac{S^f e^{-S}}{f!} exp\left[-\frac{(\Delta G + fh\upsilon + \lambda)^2}{4\lambda k_B T}\right].$$

Here we defined pre-factor $k_0 \equiv \sqrt{\pi}|V|^2/\left(\hbar\sqrt{k_B T \lambda}\right)$.

Fit of the Marcus-Jortner rate equation

^{3}MLCT lifetimes dependence from the ^{3}MLCT minimum energy was fitted using the Marcus-Jortner rate model described by Equation (4) in the main manuscript. The fit was carried out by simultaneously fitting the parameters for all three molecules. For optimization we utilized unweighted ordinary least-squares method in the $E_0^{(^3MLCT)}$ vs. ln(k) space. Results and residuals are shown in Fig. S9. In Fig. 6 these results are displayed as $E_0^{(^3MLCT)}$ vs. τ.

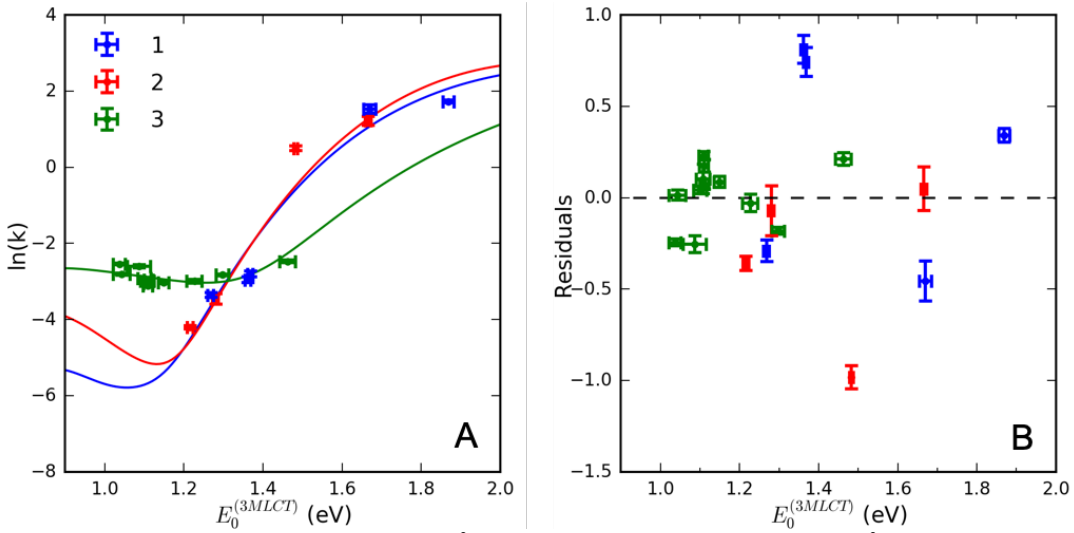

Fig. S9. (A) Simultaneous fit results of the ^{3}MLCT lifetime dependence from the ^{3}MLCT energy. (B) Residuals of the fit.

References

1 I. H. M. van Stokkum, D. S. Larsen and R. van Grondelle, *Biochim. Biophys. Acta - Bioenerg.*, 2004, **1657**, 82–104.
2 W. Gawelda, A. Cannizzo, V. T. Pham, F. van Mourik, C. Bressler and M. Chergui, *J. Am. Chem. Soc.*, 2007, **129**, 8199–8206.
3 F. Neese, *WIREs Comput Mol Sci,* 2018, 8:e1327, DOI:10.1002/wcms.1327.
4 A. D. Becke, *J. Chem. Phys.*, 1993, **98**, 5648–5652.
5 C. Lee, W. Yang and R. G. Parr, *Phys. Rev. B*, 1988, **37**, 785–789.
6 F. Weigend and R. Ahlrichs, *Phys. Chem. Chem. Phys.*, 2005, **7**, 3297.
7 D. N. Bowman and E. Jakubikova, *Inorg. Chem.*, 2012, **51**, 6011–6019.
8 V. Barone and M. Cossi, *J. Phys. Chem. A*, 1998, **102**, 1995–2001.
9 K. Kunnus, W. Zhang, M. G. Delcey, R. V. Pinjari, P. S. Miedema, S. Schreck, W. Quevedo, H. Schröder, A. Föhlisch, K. J. Gaffney, M. Lundberg, M. Odelius and P. Wernet, *J. Phys. Chem. B*, 2016, **120**, 7182–7194.
10 A. W. Hahn, B. E. Van Kuiken, V. G. Chilkuri, N. Levin, E. Bill, T. Weyhermüller, A. Nicolaou, J. Miyawaki, Y. Harada and S. DeBeer, *Inorg. Chem.*, 2018, **57**, 9515–9530.
11 Y. Tanabe and S. Sugano, *J. Phys. Soc. Jpn.*, 1954, **9**, 753–766.
12 Y. Tanabe and S. Sugano, *J. Phys. Soc. Jpn.*, 1954, **9**, 766–779.
13 F. M. F. de Groot and A. Kotani, *Core Level Spectroscopy of Solids*, CRC Press, Boca Raton, 2008.
14 R. D. Cowan, *The Theory of Atomic Structure and Spectra*, University of California Press, Berkley, 1981.
15 R. M. Jay, S. Eckert, M. Fondell, P. S. Miedema, J. Norell, A. Pietzsch, W. Quevedo, J. Niskanen, K. Kunnus and A. Föhlisch, *Phys. Chem. Chem. Phys.*, 2018, **20**, 27745–27751.
16 V. May and O. Kühn, *Charge and energy transfer dynamics in molecular systems*, Wiley-VCH, 2011.
17 M. Bixon and J. Jortner, *J. Chem. Phys.*, 1968, **48**, 715–726.
18 M. Bixon and J. Jortner, Wiley, 1999, pp. 35–202.
19 R. A. Marcus, *J. Chem. Phys.*, 1956, **24**, 966–978.
20 G. C. Walker, E. Aakesson, A. E. Johnson, N. E. Levinger and P. F. Barbara, *J. Phys. Chem.*, 1992, **96**, 3728–3736.
21 K. Tominaga, D. A. V. Kliner, A. E. Johnson, N. E. Levinger and P. F. Barbara, *J. Chem. Phys.*, 1993, **98**, 1228–1243.
22 P. J. Reid and P. F. Barbara, *J. Phys. Chem.*, 1995, **99**, 3554–3565.
23 J. Ulstrup and J. Jortner, *J. Chem. Phys.*, 1975, **63**, 4358–4368.
24 P. Siders and R. A. Marcus, *J. Am. Chem. Soc.*, 1981, **103**, 748–752.